Coherent Control to Prepare an InAs Quantum Dot for Spin-Photon Entanglement

L. A. Webster,[1] K. Truex,[1] L.-M. Duan,[1] D. G. Steel,[1,*] A. S. Bracker,[2] D. Gammon,[2] and L. J. Sham[3]
[1]*The H. M. Randall Laboratory of Physics, The University of Michigan, Ann Arbor, Michigan 48109, USA*
[2]*The Naval Research Laboratory, Washington D.C. 20375, USA*
[3]*Department of Physics, University of California, San Diego, La Jolla, California 92093-0319, USA*
(Received 26 November 2012; revised manuscript received 9 October 2013; published 24 March 2014)

We optically generated an electronic state in a single InAs/GaAs self-assembled quantum dot that is a precursor to the deterministic entanglement of the spin of the electron with an emitted photon in the proposal of W. Yao, R.-B. Liu, and L. J. Sham [Phys. Rev. Lett. **95**, 030504 (2005).]. A superposition state is prepared by optical pumping to a pure state followed by an initial pulse. By modulating the subsequent pulse arrival times and precisely controlling them using interferometric measurement of path length differences, we are able to implement a coherent control technique to selectively drive exactly one of the two components of the superposition to the ground state. This optical transition contingent on spin was driven with the same broadband pulses that created the superposition through the use of a two pulse coherent control sequence. A final pulse affords measurement of the coherence of this "preentangled" state.

DOI: 10.1103/PhysRevLett.112.126801 PACS numbers: 73.21.La, 42.50.Dv, 78.67.Hc

Quantum computation relies on controlled entanglement among the constituent bits of the quantum computer. To avoid the complication of arranging for pairs of qubits to become entangled through local interactions, many schemes call for entanglement of a bit with an intermediate photon, which would travel to another bit and entangle the two qubits [1]. The proposal of Yao, Liu, and Sham (YLS) [2] offers a deterministic method for producing such an entangled pair. The ground states of a Λ system would act as the stationary bit. Application of a pulse could coherently transfer the probability amplitude associated with one of the ground states to the excited state. Using a cavity, the density of states would be arranged to suppress decay by one of the channels, resulting in emission of a photon via the other channel. The coherent superposition of the two ground states would be converted to a superposition of one state in the absence of a photon and the other state in the presence of a photon in the cavity. This photon could be coupled to a waveguide whereby it could interact with distant stationary qubits. Such coherent control techniques have been generating interest in recent years [3,4]. Sending and receiving photons with quantum correlation with the spin states of a quantum bit of information is key to quantum telecommunication as well as for scaling up systems for quantum computation.

Here we report the creation of the state in the proposed entanglement scheme immediately prior to photon decay, the "preentangled" state, through the use of a series of picosecond laser pulses interacting with a self-assembled InAs quantum dot. Self-assembled InAs quantum dots are a favorable medium for implementation of this scheme. Their bound electronic states have long coherence times [5], have no need to be trapped, and admit fast manipulation through optically accessible excited states [6]. Despite the complexity of the fundamentally many-body nature of the interaction, an atomlike Hamiltonian pertains and coherent control of the optically excited state is possible. In contrast to previous demonstrations of coherent control in quantum dot systems, which have operated on only the stationary qubit [7,8], this work includes control of the excited states and thereby of the radiated photon. The system is comprised of the two Zeeman-split states of a single trapped electron and those of an optically excited electron-electron-hole complex (trion); Fig. 1 shows an energy level diagram. Further details concerning the system can be found in the supplemental materials [9].

The YLS protocol requires a cavity to control the final photon emission, but is not included in the current demonstration. Here the cavity dynamics are replaced with decay by interaction with the vacuum. In the procedure, based on that proposed by Truex *et al.* [10], the coherent optical excitation of the preentangled state involves first the preparation of a coherent superposition state, followed by a coherent transferal of one component of the superposition to the ground state. If the remaining component of the preentangled state could radiate into only one mode, the emitted photon would be entangled with the remaining spin. Instead, having two decay paths, our final step is to measure the coherence of the preentangled state. To reduce its complexity, this experiment is done using an initial coherent superposition in the excited state, rather than in the ground state as would be arranged in the YLS protocol. Figure 1 displays the following sequence of optical excitation.

A weak cw beam on the $|x-\rangle$ to $|t-\rangle$ transition is used to optically pump the system into the state $|x+\rangle$ [11]. Picosecond laser pulses have sufficient bandwidth to dipole-couple both ground states to both excited states and manipulate the states, thereby avoiding the need for

 © 2014 American Physical Society

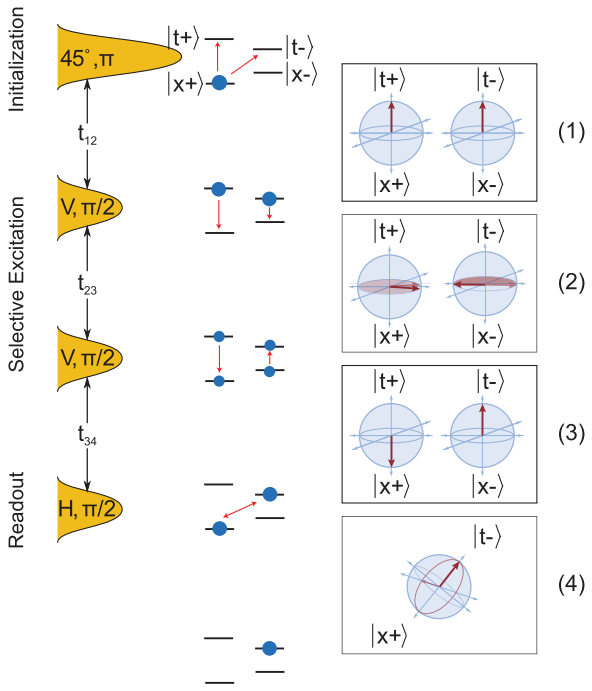

FIG. 1 (color). The four pulse process to create and measure the preentangled state, $(|x+\rangle + |t-\rangle)/\sqrt{2}$. A 45° pulse creates coherence to be transferred. Two vertical control pulses for selective excitation rely on a differential precession rate of the two Bloch vectors. A final horizontal pulse reads the resulting coherence by rotating the Bloch vector on the horizontal transition into any of several states depending on the phase of the fourth pulse.

multiple synchronized lasers. The first pulse has area π, is polarized 45°, and prepares a superposition of the two trion states (an excited state coherence). Since only one excited state is desired to emit a photon, we then need to coherently transfer the complex amplitude of one of the excited states to a ground state, but a broadband pulse cannot selectively drive this transition alone since both excited states are optically coupled to both of the spin states. Instead, selective deexcitation is accomplished using a pulse-shaping coherent control scheme [12]. Absorption in the cw beam, a, otherwise absent due to optical pumping, is recovered when the pulses transfer population out of $|x+\rangle$, and is given by the expression $a/a_\pi = \rho_{t+,t+} + \rho_{t-,t-} + 2\rho_{x-,x-}$, where a_π is the absorption signal that would result after transferring the population exclusively to the state $|t+\rangle$. Because of the sensitivity only to populations, a fourth and final pulse is employed to convert the coherence into a population to be read by the cw beam. The cw beam is on for the duration of the experiment.

To measure the coherence $\rho_{t+,t-}$ generated by the preparatory pulse, two such pulses are applied, separated by a delay t_{12}. The precession of the states is given by the upper state splitting, Δ_h. When the second pulse has the same phase as the first, the total effect is one of a 2π pulse and the population is driven back to the optically pumped state $|x+\rangle$, suppressing absorption. When it is π out of phase it is driven instead to $|x-\rangle$. The resultant signal is proportional to $\sin^2(\Delta_h t_{12}/2) = \frac{1}{2}(1 - \sin\Delta_h t_{12})$; these Ramsey fringes demonstrate the creation of excited state coherence.

To create the preentangled state, we now selectively drive the population in $|t+\rangle$ to state $|x+\rangle$, leaving that in the $|t-\rangle$ unaffected. In the YLS protocol, a cavity suppresses emission of a horizontally polarized photon and ensures that photons decay exclusively to one spin state, $|x-\rangle$. To transfer the population in the $|t+\rangle$ state to $|x+\rangle$, we follow the first pulse with two $\pi/2$ pulses, rather than a single π pulse. The two $\pi/2$ pulses must arrive on a time scale short compared to the coherence time between the two excited states. As shown in frame (1) of Fig. 1, after the preparatory pulse, one can visualize a Bloch vector for each of two two-level systems: one involving $|x+\rangle$ and $|t+\rangle$, and the other $|x-\rangle$ and $|t-\rangle$, both having vertical arrows depicting population shared equally in states $|t-\rangle$ and $|t+\rangle$. The first $\pi/2$ pulse rotates these two vectors $\pi/2$ about the horizontal axes of the spheres. They then precess about the poles of the optical Bloch spheres as shown in Fig. 1, frame (2). The coherence between the states $|t+\rangle$ and $|x+\rangle$ and that between $|x-\rangle$ and $|t-\rangle$ both precess at the optical frequency, but due to the splitting, the precession rate of the latter coherence is slower and lags the former. The difference in rates is just the sum of the electron and hole splitting, $\Delta_e + \Delta_h$. If the second $\pi/2$ pulse arrives when a phase lag of π has accumulated, the rotation of $\pi/2$ about z moves the first Bloch vector down as it sends the second back up, so that the effect of the two control pulses is to coherently move the population in $|t+\rangle$ down without affecting the population in $|t-\rangle$. By precisely timing the pulses, we can create the preentangled state, $|\psi_{\mathrm{PE}}\rangle = (|x+\rangle + |t-\rangle)/\sqrt{2}$ [frame (3) of Fig. 1]. These first three pulses, in the limit of infinite pulse bandwidth and no decay or cw beam, give rise to a measured absorption varying as $a/a_\pi = 1 + \frac{1}{2}\sin((\Delta_e + \Delta_h/2)t_{23})\sin\omega t_{23}$, which reflects the relatively slow precession of the excited state coherence as the time delay maps the accumulating phase lag between the two optical Bloch vectors. The optical frequency ω corresponds to the average of the two transition frequencies.

The absorption also varies with delay between the control pulses t_{23} at the optical frequency, ω, and the state created is likewise sensitive to the arrival time of the second control pulse—to wait just one half optical cycle would generate the state $(|x-\rangle + |t+\rangle)/\sqrt{2}$, instead. This requires precision in the pulse delay of much less than a single optical period. To achieve this precision, we use a passively stabilized Michelson interferometer.

The inset of Fig. 2 shows a representative data set collected using this method. The Ramsey fringe associated with the $\sin\omega t_{23}$ in the absorption is clear. The lag in the precession rates of the two Bloch vectors leads to the

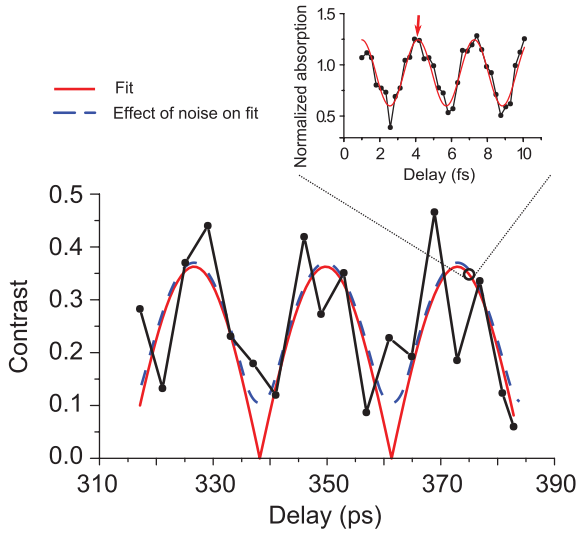

FIG. 2 (color). Fringe contrast vs delay t_{23}. Following initialization by optical pumping, a Ramsey fringe appears in the absorption as a function of delay t_{23} between the two control pulses. An example fringe is displayed in the inset. For each scan, an amplitude and offset are extracted and to plot contrast against coarse delay. The red, solid line is the best fit to the absolute value of the sin function, and the blue, dashed line is the expected value of the fitted fringe amplitudes given the noise. The red arrow in the inset indicates a time delay where the preentangled state $|\psi_{\mathrm{PE}}\rangle = (|x+\rangle + |t-\rangle)/\sqrt{2}$ is created.

anticipated modulation of the fringe amplitude, as seen in the three-pulse absorption signal. By taking several such data sets at various time delays and plotting the normalized amplitude of the Ramsey fringe, we trace out this envelope function as shown in Fig. 2. Fitting this function to the data yields a period of 21 ps, which closely matches the value of 24 ps expected from the splitting of the absorption peaks. Ideally we would see a cusp in the amplitude as it crossed through zero, but noise in each trace has a component with a random phase that adds to the true amplitude. The dashed, blue line in Fig. 2 shows the expected value of the magnitude of the sum given the amplitude of the noise and averaging over the phase.

From the behavior of the populations as a function of arrival time of the second control pulse, the preentangled state occurs at the point indicated by the arrow in the inset of Fig. 2, the delay giving maximum signal and maximum contrast. For useful quantum entanglement, it is necessary that the quantum coherence be maintained between the states reflecting the quantum superposition, not just the proper eigenstate probabilities. Since the detection method is sensitive to populations only, not to coherences, we apply a fourth pulse to rotate the coherence into a population.

We fix the first three pulse delays, with the delay between the second and third pulse actively locked using the side of a HeNe fringe. This generates a coherence to be read, which precesses at the optical frequency. A new Bloch

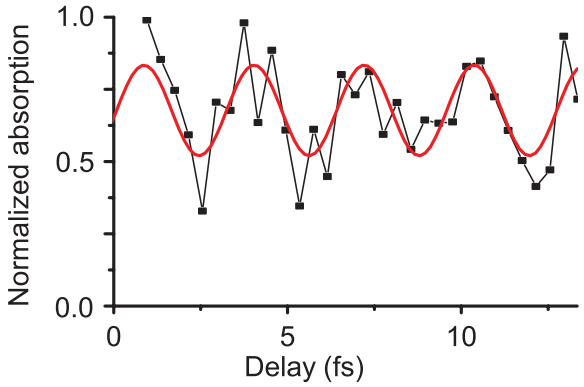

FIG. 3 (color). Presence of oscillation in the signal as a function of arrival time of the readout pulse indicates coherence between the $|x+\rangle$ and $|t-\rangle$ states that is present after the preparatory and selective excitation pulses. The solid red line is the best sinusoid fit to the data points.

vector can be visualized [frame (4) of Fig. 1], using states $|x+\rangle$ and $|t-\rangle$, with the oscillating coherence represented by the precession of the Bloch vector on the equator of the sphere. The fourth pulse, with area $\pi/2$, now strikes the system at some point in its precession, driving it fully into state $|x+\rangle$, to $|t-\rangle$, or to a superposition of the two depending on its precise arrival time. Therefore, by scanning the arrival time of the readout pulse, we generate a sinusoidal signal confirming the coherence, whose amplitude measures the magnitude of the coherence present at its arrival, as shown in Fig. 3. The contrast here is 0.23.

Making no assumptions about the action of the first three pulses, but assuming the fourth pulse is a $\pi/2$ pulse for both horizontal transitions results in the following expression for the signal in the four pulse experiment, expressed in terms of the density matrix elements immediately prior to the fourth pulse: $a/a_\pi = \frac{1}{2} + \rho_{x-,x-} + \rho_{t+,t+} + |\rho_{x+,t-} + \rho_{x-,t+}| \sin(\omega t_{34} + \phi)$. The third term oscillates in time at the optical frequency and reports on the coherence of the preentangled state $\rho_{x+,t-}$, as well as the coherence $\rho_{x-,t+}$, which has been designed to be zero in this demonstration. The time t_{34} is the delay between pulses 3 and 4, and ϕ an undetermined phase. From our data and the fact that $\mathrm{Tr}\,\rho = 1$ we find $\rho_{x-,x-} + \rho_{t+,t+} = 0.11 \pm 0.03$, $\rho_{x+,x+} + \rho_{t-,t-} = 0.89 \pm 0.03$, and $|\rho_{x+,t-} + \rho_{x-,t+}| = 0.16 \pm 0.03$. The density matrix elements here are determined immediately before the fourth pulse. Accounting for the fact that some decay occurs during the interval between the third and fourth pulses and noting that maximum coherence between two levels results when the populations are equally balanced and coherent with one another, we find the following constraints on the density matrix elements immediately after the third pulse: $|\rho_{x+,t-}| \le 2(0.89)/3 + e^{-\gamma_2 t_{34}} = 0.46$, $|\rho_{x-,t+}| \le 2(0.11)/3 + e^{-\gamma_2 t_{34}} = 0.06$, and $|\rho_{x+,t-} + \rho_{x-,t+}| = 0.16 e^{\gamma t_{34}} = 0.29$. The rate γ_2 is the decay rate of the excited state populations, and γ that of the coherence between excited

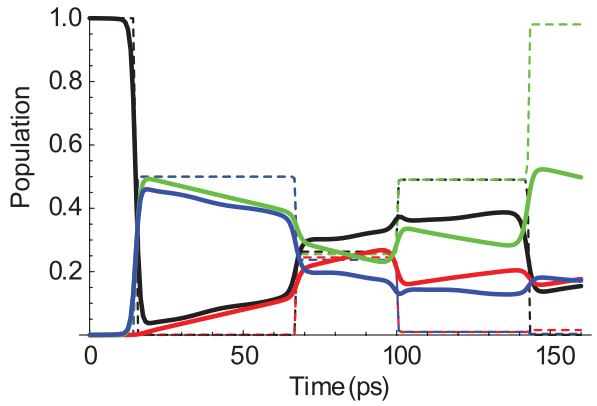

FIG. 4 (color). Populations as a function of time. Solid black, red, green, and blue lines, are for populations in $|x+\rangle$, $|x-\rangle$, $|t-\rangle$, and $|t+\rangle$, respectively. Corresponding dashed lines show the ideal case in absences of the cw beam and decay, and with a large bandwidth. After the third pulse the system is to be in an equal, coherent superposition of the states $|x+\rangle$ and $|t-\rangle$. The fidelity of the transformation is 0.81, reduced mainly due to decay during the pulse sequence.

and ground states, 2.2 and 7.6 ns^{-1}, respectively. These constraints, together with the triangle inequalities, result in $0.23 \leq |\rho_{x+,t-}| \leq 0.35$ and $0 \leq |\rho_{x-,t+}| \leq 0.06$, with a statistical error of 0.02. Under ideal conditions the values of the coherences $\rho_{x+,t-}$ and $\rho_{x-,t+}$ would be 0.5 and 0, respectively.

To ascertain the main sources of deviation from ideal behavior, we have computed the time evolution of the density matrix using a full numerical simulation that accounts for the decay and decoherence as well as for the finite pulse widths and the presence of the cw beam. The supplement includes details about the simulation, and an example its output is shown in Fig. 4. Under conditions of the experiment, decay rates as cited above, a cw Rabi frequency of 1.6 GHz, and pulse duration (field FWHM) 4 ps, we find the normalized simulated amplitude of the Ramsey fringe to be 0.16, in close agreement with both the observed value (0.16) and the magnitude of the sum of the simulated coherences, accounting for decay between the third and fourth pulses (0.18). This is an indication of the reliability of the estimate of coherence given the measured amplitude. Furthermore, the coherence estimate given the data is comparable to the computed coherence of $|\rho_{x+,t-}| = 0.30$ and $|\rho_{x-,t+}| = 0.03$

To estimate the fidelity, F of the final state to the intended preentangled state, $|\psi_{\mathrm{PE}}\rangle$, we use the simulated final state as a proxy. The preentangled state being a pure state, we may write [13] $F = \sqrt{\langle\psi_{\mathrm{PE}}|\rho|\psi_{\mathrm{PE}}\rangle} = 0.81$. In the uniformly mixed case the fidelity would be 0.5, while the ideal value is 1. The fidelity falls short of unity for a number of reasons: Decay between the pulses transfers population from the upper states to the ground states and destroys the coherences. Also during this time the cw readout and initialization beam is on, which alters both populations and coherences. The splitting also prevents the pulses from being resonant with all transitions. The finite pulse bandwidth, therefore, causes the pulses to affect each transition slightly differently. We conclude that loss of fidelity is primarily due to decay, the cw Rabi flopping and the finite bandwidth each reducing fidelity by only 0.01. The delay t_{12} can be reduced to mitigate the effects of decay, but the splittings determine the minimum t_{23}: half the period of the peaks in Fig. 2, around 12 ps. Simulations suggest that under the current conditions, the fidelity of the operation could be improved to 0.93 by reduction of t_{12}, and reduction of t_{23} to the minimum. Shorter delays t_{23} would require a higher magnetic field and a wider pulse bandwidth. On the other hand, larger pulse bandwidths could begin to excite higher lying transitions in the dot or nearby states in the structure. Further studies would be needed to evaluate this.

We can also use the computed density matrix to compute the entropy of entanglement of the spin-photon state if the state that we observe were generated in a cavity as described above. The entanglement between the photon number and electron spin as computed by the formula of Wooters [14] and assuming decay from $|t-\rangle$ exclusively to $|x-\rangle$, would be 0.18, again primarily limited by decay. Reducing the delay t_{12} could increase the entanglement to 0.60.

In summary, we have approximated ($F = 0.81$) a state that would deterministically lead to entanglement of an electron spin in a quantum dot with a propagating photon. The experimental demonstration is a step toward overcoming the challenges of managing a quantum messenger that is entangled with a local qubit and can be further used to entangle either another messenger or a distant stationary qubit. We employ an interferometric technique to achieve the femtosecond level precision that the coherent control demands. The same technique applied to the final pulse enables detection of the coherence of the pre-entangled state, which we find to be 0.29.

We would like to acknowledge the support of the ARO, AFOSR, NSF, ONR, and DARPA.

*dst@umich.edu

[1] D. P. Divincenzo, in *The Physical Implementation of Quantum Computation, Scalable Quantum Computers: Paving the Way to Realization, edited by S. L. Braunstein, H.-K. Lo, and P. Kok (Wiley-VCH Verlag GmbH & Co. KGaA, Weinheim, 2005).*
[2] W. Yao, R.-B. Liu, and L. J. Sham, Phys. Rev. Lett. **95**, 030504 (2005).
[3] A. J. Ramsay, Semicond. Sci. Technol. **25**, 103001 (2010).
[4] S. Spatzek, A. Greilich, S. E. Economou, S. Varwig, A. Schwan, D. R. Yakovlev, D. Reuter, A. D. Wieck, T. L. Reinecke, and M. Bayer, Phys. Rev. Lett. **107**, 137402 (2011).

[5] M. Kroutvar, Y. Ducommun, D. Heiss, M. Bichler, D. Schuh, G. Abstreiter, and J. J. Finley, Nature (London) **432**, 81 (2004).
[6] J. Berezovsky, M. H. Mikkelsen, N. G. Stoltz, L. A. Coldren, and D. D. Awschalom, Science **320**, 349 (2008).
[7] E. D. Kim, K. Truex, X. Xu, B. Sun, D. G. Steel, A. S. Bracker, D. Gammon, and L. J. Sham, Phys. Rev. Lett. **104**, 167401 (2010).
[8] V. Jovanov, F. Klotz, S. Kapfinger, D. Heiss, S. Spiga, D. Rudolph, M. Bichler, M. S. Brandt, G. Abstreiter, and J. J. Finley, SPIE Proc. **8272**, 827211 (2012).
[9] See Supplemental Material at http://link.aps.org/supplemental/10.1103/PhysRevLett.112.126801 for further information including system and experimental details, as well as more information about the modeling procedure.
[10] K. Truex, L. A. Webster, L.-M. Duan, L. J. Sham, and D. G. Steel, Phys. Rev. B **88**, 195306 (2013).
[11] X. Xu, Y. Wu, B. Sun, Q. Huang, J. Cheng, D. G. Steel, A. S. Bracker, D. Gammon, C. Emary, and L. J. Sham, Phys. Rev. Lett. **99**, 097401 (2007).
[12] C. Piermarocchi, P. Chen, Y. S. Dale, and L. J. Sham, Phys. Rev. B **65**, 075307 (2002).
[13] M. A. Nielsen and I. L. Chuang, *Quantum Computation and Quantum Information (Cambridge University Press, Cambridge, England, 2010)*.
[14] W. K. Wootters, Phys. Rev. Lett. **80**, 2245 (1998).